Article

Discovery Medicine 2026; 38(207): 1163–1179
https://doi.org/10.24976/Discov.Med.202638207.93

SRSF1 Expression in the Endometrial Carcinoma Microenvironment: Association With Macrophage Efferocytosis and Implications for Tumor Progression

Ao Zhang[1], Yang Gao[1], Rui Fang[2], Zheng Li[2], Qing Zhu[3,4,*]

[1]The Graduate School, Bengbu Medical University, 233030 Bengbu, Anhui, China
[2]The Graduate School, The First Affiliated Hospital of Bengbu Medical University, 233004 Bengbu, Anhui, China
[3]Department of Pathology, Bengbu Medical University, 233030 Bengbu, Anhui, China
[4]Department of Pathology, The First Affiliated Hospital of Bengbu Medical University, 233004 Bengbu, Anhui, China
*Correspondence: 2014012@bbmu.edu.cn (Qing Zhu)
Submitted: 27 November 2025 Revised: 11 February 2026 Accepted: 19 March 2026 Published: 20 April 2026

Background: Serine/arginine-rich splicing factor 1 (*SRSF1*) is a critical RNA splicing regulator implicated in various cancer types. However, its cell-type-specific expression patterns and functions within the tumor microenvironment remain poorly understood, particularly its interaction with immune cell populations. This study aimed to investigate *SRSF1* expression patterns across different cell types in the endometrial carcinoma microenvironment using single-cell RNA sequencing and explore its potential association with macrophage efferocytosis.

Methods: We analyzed single-cell RNA sequencing data from five endometrial carcinoma samples (GSE173682, n = 33,178 cells) to characterize *SRSF1* expression patterns. Efferocytosis activity was assessed using gene signature scoring with the AUCell algorithm. Cell-cell communication networks were analyzed using CellChat to identify interaction patterns. *SRSF1* expression was validated in bulk tissue datasets from The Cancer Genome Atlas (TCGA) and Clinical Proteomic Tumor Analysis Consortium (CPTAC). Functional validation studies were performed in the Ishikawa endometrial cancer cell line using lentiviral-mediated *SRSF1* knockdown.

Results: Single-cell analysis revealed significantly elevated *SRSF1* expression in tumor-associated macrophages compared to other cell types ($p < 0.05$), with moderate expression also detected in tumor epithelial cells. Spatial analysis demonstrated a strong overlap between regions of high *SRSF1* expression and areas exhibiting elevated efferocytosis activity. Functional enrichment analysis showed that efferocytosis-related genes participate in immune responses, extracellular activities, and antigen processing pathways. Pseudotime trajectory analysis identified seven functionally distinct macrophage subpopulations, including pro-inflammatory (M1-like) and immunosuppressive (M2-like) phenotypes, with varying *SRSF1* expression levels. Cell-cell communication analysis revealed extensive interactions between macrophages and other cell types through specific ligand-receptor pairs, including *SPP1-CD44*. Bulk tissue analysis confirmed *SRSF1* upregulation in endometrial carcinoma at both mRNA (TCGA, $p < 0.05$) and protein (CPTAC, $p < 0.05$) levels. *In vitro* functional validation in the Ishikawa cell line demonstrated that *SRSF1* knockdown significantly inhibited cell proliferation (30–40% reduction at 96 hours), migration, invasion, and modulated epithelial-mesenchymal transition markers.

Conclusion: This study reveals cell-type-specific *SRSF1* expression patterns in the endometrial carcinoma microenvironment and demonstrates strong associations between *SRSF1* and macrophage efferocytosis activity. Correlation analysis showed significant associations between *SRSF1* and key efferocytosis receptors (Mer tyrosine kinase (*MERTK*)), growth arrest-specific protein 6 (*GAS6*), providing molecular evidence for *SRSF1*'s involvement in macrophage function.

Keywords: *SRSF1*; endometrial carcinoma; tumor microenvironment; single-cell RNA sequencing; macrophage efferocytosis; tumor-associated macrophages

Introduction

Endometrial carcinoma (EC) remains one of the most common gynecological malignancies worldwide. According to the latest GLOBOCAN 2020 estimates, approximately 417,367 new cases were diagnosed globally, with 97,370 disease-related deaths [1]. The incidence continues to rise, particularly in developed countries, driven by aging populations and increasing rates of obesity and metabolic syndrome [2]. While early-stage endometrial carcinoma has a favorable prognosis, with 5-year survival rates exceeding 95%, patients with advanced or recurrent disease have limited treatment options and poor outcomes [3,4], with 5-year survival rates of only 20–26% for stage IV disease [3]. Therefore, elucidating the molecular mechanisms

underlying endometrial carcinoma pathogenesis and progression is crucial for developing more effective diagnostic and therapeutic strategies. Serine/arginine-rich splicing factor 1 (*SRSF1*, also known as ASF/SF2) is a core member of the SR protein family that plays essential roles in constitutive and alternative splicing, as well as in mRNA export, stability, and translation [5]. *SRSF1* functions as a sequence-specific splicing regulator that binds to exonic splicing enhancers and promotes exon inclusion [6]. Recent studies have identified *SRSF1* as a proto-oncogene, with aberrant expression documented across various cancer types, including breast, lung, colon, and liver cancers [7–9]. Elevated *SRSF1* expression has been shown to promote tumor cell proliferation, inhibit apoptosis, and enhance invasion and metastasis through regulating cancer-relevant alternative splicing events [10,11]. Additionally, *SRSF1* has been implicated in the regulation of microRNA biogenesis, expanding its potential roles in gene expression control [12]. However, the specific expression patterns and functional roles of *SRSF1* within the complex tumor microenvironment, particularly its relationship with immune cell functions, remain largely unexplored. The tumor microenvironment (TME) represents a complex ecosystem comprising diverse cell types, including malignant cells, immune cells, stromal cells, and vascular endothelial cells, which collectively influence tumor behavior [13]. Among immune cell populations, tumor-associated macrophages (TAMs) are typically the most abundant and play multifaceted, context-dependent roles in tumor initiation, progression, angiogenesis, and response to therapy [14,15]. Recent evidence suggests that targeting splicing factors, including *SRSF1*, can modulate immune cell function and enhance cancer immunotherapy efficacy [16]. Macrophages perform the specialized function of efferocytosis—the recognition and clearance of apoptotic cells—which is essential for maintaining tissue homeostasis and resolving inflammation [17]. Notably, efferocytosis by tumor-associated macrophages is often dysregulated within the tumor microenvironment, with significant implications for tumor progression [18]. Efferocytosis is a tightly regulated process that, under physiological conditions, prevents inflammation by efficiently clearing dying cells before they undergo secondary necrosis [19]. However, within the tumor immune microenvironment, efferocytosis plays paradoxical roles: while efficient clearance of apoptotic tumor cells might reduce pro-inflammatory signals, it can simultaneously induce immunosuppressive phenotypes in macrophages, potentially facilitating tumor immune evasion and progression [20,21]. Despite growing interest in this area, the molecular mechanisms governing efferocytosis in the tumor microenvironment and its relationship with splicing regulation remain poorly defined. The advent of single-cell RNA sequencing (scRNA-seq) technology has revolutionized our ability to dissect tumor microenvironment complexity at unprecedented resolution [22]. By profiling transcriptomes at the single-cell level, researchers can identify cell-type-specific gene expression signatures, discover rare cell populations, and map intricate cell-cell interaction networks [23]. Recent scRNA-seq studies have revealed that *SRSF1* governs cell-type-specific alternative splicing programs essential for tissue homeostasis and cellular differentiation [24]. However, comprehensive single-cell analysis of *SRSF1* expression patterns in endometrial carcinoma and its potential involvement in immune cell functions has not been reported. In this study, we leveraged single-cell RNA sequencing data to systematically investigate *SRSF1* expression patterns across different cell types in the endometrial carcinoma microenvironment and explore its potential association with macrophage efferocytosis. We discovered that *SRSF1* is preferentially expressed in tumor-associated macrophages and strongly correlates with efferocytosis activity. Furthermore, through pseudotime trajectory analysis, cell-cell communication network mapping, and functional validation experiments in the Ishikawa endometrial cancer cell line, we provide evidence that *SRSF1* may participate in regulating macrophage functional states while also directly affecting tumor cell behavior. These findings offer novel insights into the multifaceted roles of *SRSF1* in the tumor immune microenvironment and suggest its potential as both a biomarker and a therapeutic target in endometrial carcinoma.

Materials and Methods

Bulk Tissue Database Analysis

SRSF1 expression data from bulk tumor tissues were obtained from The Cancer Genome Atlas (TCGA) database [25] and The Clinical Proteomic Tumor Analysis Consortium (CPTAC) database [26]. For pan-cancer analysis, differential expression analysis was performed comparing tumor tissues to normal tissues across 33 cancer types using the TCGA dataset. For endometrial carcinoma (UCEC), we analyzed CPTAC proteomic data to assess protein-level expression and TCGA dataset to evaluate mRNA expression in unpaired samples, with additional validation performed using matched-paired samples. Differential expression was assessed using Wilcoxon rank-sum tests for unpaired samples and Wilcoxon signed-rank tests for paired samples. The diagnostic potential of *SRSF1* was evaluated using receiver operating characteristic (ROC) curve analysis, with the area under the curve (AUC) calculated using the pROC package (CRAN, https://cran.r-project.org) in R [27]. For pan-cancer differential expression analysis across 33 cancer types, Wilcoxon rank-sum tests were independently performed comparing tumor tissues with normal tissues for each cancer type. p-values were adjusted for multiple comparisons using the Benjamini-Hochberg method, with adjusted $p < 0.05$ considered statistically significant.

Data Acquisition and Processing

This study analyzed the GSE173682 dataset from the Gene Expression Omnibus (GEO) database, originally generated by Regner *et al*. [28], which contains single-cell RNA sequencing data from five endometrial adenocarcinoma samples. The dataset comprised 35,868 cells, of which 33,178 passed quality control filtering and were retained for subsequent analysis. The distribution of cells across the five tumor samples was as follows: tumor1 (5218 cells), tumor2 (7128 cells), tumor3 (5323 cells), tumor4 (7747 cells), and tumor5 (7762 cells).

Quality Control and Data Normalization

We implemented stringent quality-control parameters for cell filtering based on standard scRNA-seq practices: number of detected genes per cell (50 $<$ nFeature_RNA $<$ 7500), total RNA counts per cell (100 $<$ nCount_RNA $<$ 50,000), and percentage of mitochondrial gene expression ($<$20%). Quality-control analysis revealed a negative correlation between total RNA counts and mitochondrial gene percentage (r = –0.17) and a strong positive correlation between RNA counts and number of detected genes (r = 0.9), indicating high-quality data. Data normalization was performed using the SCTransform method from the SeuratR package (version 4.3.0) [29] (Satija Lab, New York Genome Center, New York, NY, USA). SCTransform was chosen over traditional log-normalization methods for several reasons. First, it effectively models the relationship between mean expression and variance using regularized negative binomial regression, thereby removing technical variation while preserving biological heterogeneity. Second, unlike standard log-normalization, which applies the same transformation to all genes, SCTransform accounts for gene-specific technical effects, making it particularly suitable for datasets with heterogeneous cell types such as the tumor microenvironment. Third, it obviates the need for separate scaling and variable gene selection steps by outputting Pearson residuals that are directly comparable across genes. This approach has been shown to improve downstream analyses, particularly for datasets with high technical noise or batch effects [29]. In our analysis, SCTransform improved cell type separation and cluster resolution in UMAP visualization compared to traditional log-normalization. Highly variable genes (HVGs) were identified using the FindVariableFeatures function in Seurat with the "vst" (variance stabilizing transformation) method. The top 2000 most variable genes were selected based on standardized variance for subsequent analyses, including principal component analysis and clustering. For dimensionality reduction and visualization, we employed principal component analysis (PCA) using the top 2000 HVGs, followed by Uniform Manifold Approximation and Projection (UMAP) with default parameters (n_neighbors = 30, min_dist = 0.3, metric = "cosine"). For dimensionality reduction and visualization, principal component analysis (PCA) followed by Uniform Manifold Approximation and Projection (UMAP) was employed with default parameters.

Cell Clustering and Type Annotation

Cell clustering was performed using the FindClusters function in Seurat with a resolution parameter of 1.0, resulting in the identification of 26 distinct clusters (cluster 0 through cluster 25). Cell type annotation was achieved through a combination of manual curation based on canonical marker gene expression and comparison with established cell type signatures.

The following marker genes were used for cell type identification:

- Tumor epithelial cells: *EPCAM*, *KRT8*, *KRT18*, *KRT19*, *MUC1*
- Vascular endothelial cells: *PECAM1* (CD31), *VWF*, *CDH5*, *CLDN5*
- Lymphatic endothelial cells: *PROX1*, *LYVE1*, *PDPN* (Podoplanin)
- T cells: *CD3D*, *CD3E*, *CD4*, *CD8A*, *CD8B*
- Macrophages: *CD68*, *CD163*, *CD14*, *FCGR3A* (CD16), *CSF1R*
- Fibroblasts: *COL1A1*, *COL1A2*, *DCN*, *LUM*, *FAP*
- Mesenchymal stem cells: *CD44*, *THY1* (CD90), *ENG* (CD105), *NT5E* (CD73)
- Smooth muscle cells: *ACTA2*, *MYH11*, *TAGLN*, *CNN1*
- Mast cells: *TPSAB1*, *CPA3*, *KIT* (CD117), *HPGDS*

Cell type assignments were validated by examining multiple markers per cell type and comparing expression patterns with published endometrial tissue single-cell atlases [30,31].

SRSF1 Expression Analysis

SRSF1 expression patterns were visualized using dot plots and UMAP projections generated with Seurat functions. Correlation analyses were performed using two methods depending on data type: Pearson correlation coefficients were used for bulk tissue mRNA expression data from TCGA-UCEC to assess correlations between *SRSF1* and efferocytosis-related genes Mer tyrosine kinase (*MERTK*), *AXL* receptor tyrosine kinase (*AXL*), tyrosine-protein kinase receptor *TYRO3* (*TYRO3*), and growth arrest-specific protein 6 (*GAS6*). Spearman correlation was used for single-cell RNA sequencing data to account for non-normal distributions and potential outliers inherent to sparse single-cell datasets. Statistical comparisons of *SRSF1* expression levels between different cell types were performed using the Kruskal-Wallis test followed by Dunn's post-hoc test with Bonferroni correction for multiple comparisons. A p-value threshold of 0.05 was considered statistically significant. Visualization of gene expression patterns was performed using multiple complementary approaches: dot plots generated with DotPlot function showing both the

percentage of expressing cells (dot size) and average expression levels (color intensity), violin plots using VlnPlot function displaying the distribution of expression values across cell types, and feature plots using FeaturePlot function overlaying expression values on UMAP coordinates to show spatial patterns. Heatmaps were generated using either Seurat's DoHeatmap function for integrated Seurat objects or the ComplexHeatmap package (version 2.12.0, Bioconductor, https://bioconductor.org) for customized visualizations. All figures were created using Seurat's built-in functions (version 4.3.0) or ggplot2 (version 3.4.0,Tidyverse, https://ggplot2.tidyverse.org) in R.

Efferocytosis Scoring and Functional Enrichment Analysis

We constructed an efferocytosis gene signature based on genes involved in apoptotic cell recognition, engulfment, and processing, compiled from published literature [19–21]. The gene list included receptors (e.g., *MERTK*, *AXL*, *TYRO3*, *CD36*, *SCARF1*), bridging molecules (e.g., *GAS6*, *PROS1*, MFG-E8/*MFGE8*, C1Q), and downstream signaling components.

Efferocytosis activity scoring for all cells was performed using the AUCell package (version 1.18.0) (Bioconductor, https://bioconductor.org) [32], which calculates the Area Under the Curve (AUC) for gene set enrichment. The threshold of AUC $>$ 0.073 for defining high efferocytosis activity was determined by examining the distribution of efferocytosis scores across all cells and identifying a biologically meaningful cutoff that separated cells with substantial efferocytosis-related transcriptional activity from those with minimal activity. Cells exceeding this threshold were designated as having high efferocytosis activity, consistent with established definitions of efferocytosis as a critical process in apoptotic cell clearance and immune regulation [19,20]. This threshold was chosen to capture approximately 78% of cells (25,841 out of 33,178) showing elevated efferocytosis gene expression signatures. To identify overlapping genes between cell type markers and the efferocytosis gene signature, Venn diagram analysis was performed. Cell type marker genes were identified using the FindAllMarkers function in Seurat with the following parameters: minimum percentage of cells expressing the gene (min.pct = 0.25), minimum log fold-change threshold (logfc.threshold = 0.25), and Wilcoxon rank-sum test for differential expression. The intersection of marker genes and efferocytosis-related genes was calculated and visualized using the VennDiagram package (version 1.7.3, CRAN, https://cran.r-project.org) in R. Gene Ontology (GO) enrichment analysis (Biological Process, Cellular Component, and Molecular Function) and Kyoto Encyclopedia of Genes and Genomes (KEGG) pathway analysis were conducted on efferocytosis-related genes using the clusterProfiler package (version 4.4.0, Bioconductor, https://bioconductor.org) [33]. Significantly enriched terms were identified using adjusted p-value < 0.05 (Benjamini-Hochberg correction).

Macrophage Subpopulation Analysis

To investigate macrophage polarization states, M1 and M2 signature scores for all macrophage cells were calculated. M1 markers included *IL1B*, *TNF*, *CXCL9*, *CXCL10*, *IL6*, *NOS2*, *CD86*, while M2 markers included *CD163*, *MRC1* (CD206), *ARG1*, *IL10*, *TGFB1*, *CCL18*, *CD209*. Module scores were calculated using the AddModuleScore function in Seurat.

Pseudotime Trajectory Analysis

Pseudotime trajectory analysis was performed using the Monocle 2 R package (version 2.24.0, Bioconductor, https://bioconductor.org) [34,35] to explore macrophage differentiation trajectories. Macrophage cells were extracted from the full dataset, and dimensionality reduction was performed using the DDRTree (Discriminative Dimensionality Reduction via Learning a Tree) method. Cell ordering along pseudotime was determined using the orderCells function, with the root state defined based on the expression of early macrophage markers. Gene expression dynamics along the pseudotime trajectory were visualized using the plot_genes_in_pseudotime and plot_genes_branched_heatmap functions.

Cell-Cell Communication Analysis

Cell-cell communication networks were analyzed using the CellChat R package (version 1.6.0, GitHub, https://github.com/sqjin/CellChat) [36], which infers biologically significant cell-cell interactions from scRNA-seq data based on known ligand-receptor pairs. CellChat was analyzed using the human ligand-receptor interaction database with default parameters. The number and strength of interactions between cell types were quantified, and specific ligand-receptor pairs were identified and visualized using CellChat's built-in functions, including netVisual_circle and netVisual_heatmap.

Cell Culture

The human endometrial carcinoma cell line Ishikawa (Type I, well-differentiated endometrioid adenocarcinoma, Cat# C5504) was obtained from Hangzhou Biomat Biotech Co., Ltd. (BDBIO, Hangzhou, China). Cells were cultured in high-glucose Dulbecco's Modified Eagle Medium (DMEM; Cat# L100-500, BDBIO, Hangzhou, China) supplemented with 10% fetal bovine serum (FBS; Cat# F801-500, BDBIO, Hangzhou, China) and 1% penicillin-streptomycin (Cat# ST488, Beyotime, Shanghai, China). Cells were maintained in a humidified incubator (Heracell™ VIOS 160i CO_2 Incubator, Model 51026280, Thermo Fisher Scientific, Waltham, MA, USA) at 37 °C with 5% CO_2. Cells were passaged every 2–3 days using 0.25% Trypsin-EDTA solution (Cat# T1320-100, BDBIO,

Hangzhou, China) at a ratio of 1:3–1:6, and cells used in experiments were within passage 15. Cell line authentication was performed using short tandem repeat (STR) profiling (performed by Shanghai Zhongke Life Sciences Co., Ltd.), and mycoplasma testing was conducted regularly using PCR-based detection (MycoBlue™ Mycoplasma Detector, Cat# D101, Vazyme, Nanjing, China), and all cell lines tested negative for mycoplasma contamination throughout the study.

SRSF1 Knockdown

Stable *SRSF1*-knockdown cells were established using lentiviral-mediated shRNA delivery. Three groups were established: NC (blank control), sh-NC (scrambled control), and sh-*SRSF1* (*SRSF1* knockdown). Lentiviral shRNA plasmids (pLKO.1-puro backbone) targeting human *SRSF1* (NM_006924.4) were designed and synthesized by Shanghai GeneChem Co., Ltd. (GeneChem, Shanghai, China). The shRNA target sequences were as follows:

sh-NC: 5′-TTCTCCGAACGTGTCACGT-3′ (non-targeting scrambled control, Addgene #40625);

sh-*SRSF1*: 5′-GCAGCAAGATACGAACCAT-3′ (targeting *SRSF1* CDS region).

RNA Extraction and RT-qPCR

Total RNA was extracted using TRIzol reagent (Cat# 15596026, Lot# 2345678A, Invitrogen, Carlsbad, CA, USA) according to the manufacturer's protocol. RNA quality and quantity were assessed using a NanoDrop spectrophotometer (NanoDrop 2000c, Thermo Fisher Scientific, Waltham, MA, USA). First-strand cDNA was synthesized from 1 µg total RNA using the PrimeScript RT Reagent Kit (Cat# RR037A, Lot# AK9801, Takara Bio, Kusatsu, Japan). Quantitative real-time PCR (RT-qPCR) was performed using SYBR Green PCR Master Mix (Cat# 4309155, Lot# 2234567B, Applied Biosystems, Foster City, CA, USA) on a QuantStudio 3 Real-Time PCR System (Thermo Fisher Scientific). β-actin served as the internal reference gene. Primer sequences were as follows:

- *SRSF1*-Forward: 5′-TCTACTGACAGCCCCTTGGT-3′
- *SRSF1*-Reverse: 5′-ACTTCCAACTATGATTAGCACCCA-3′
- β-actin-Forward: 5′-TGGCACCCAGCACAATGAA-3′
- β-actin-Reverse: 5′-CTAAGTCATAGTCCGCCTAGAAGCA-3′

Relative gene expression was calculated using the $2^{-\Delta\Delta Ct}$ method. All experiments were performed in triplicate and repeated at least three times independently.

Western Blot Analysis

Cells were lysed in RIPA buffer (Cat# P0013B, Beyotime, Shanghai, China) containing 1 mM PMSF (Cat# ST506, Beyotime) and phosphatase inhibitor cocktail (Cat# 04906837001, Roche Diagnostics, Basel, Switzerland) at 4 °C for 30 min. After centrifugation at 12,000 ×g for 15 min at 4 °C, protein concentrations were determined using the BCA Protein Assay Kit (Cat# P0012, Beyotime). Equal amounts of protein (30 µg) were separated by 10% *SDS*-PAGE (Mini-PROTEAN® Tetra Cell, Cat# 1658004, Bio-Rad, Hercules, CA, USA) and transferred onto 0.45 µm PVDF membranes (Cat# ISEQ00010, Millipore, Burlington, MA, USA) at 300 mA for 90 min at 4 °C. Membranes were blocked with 5% non-fat milk (Cat# 232100, BD Difco, Sparks, MD, USA) in TBST for 1 h at room temperature, then incubated overnight at 4 °C with primary antibodies: β-actin (1:50,000, Cat# 66009-1-Ig, mouse monoclonal, Proteintech, Wuhan, China), *SRSF1* (1:1000, Cat# 12929-2-AP, rabbit polyclonal, Proteintech), E-cadherin (1:5000, Cat# 20874-1-AP, rabbit polyclonal, Proteintech), N-cadherin (1:5000, Cat# 22018-1-AP, rabbit polyclonal, Proteintech), and Vimentin (1:10,000, Cat# 10366-1-AP, rabbit polyclonal, Proteintech). After washing with TBST (3 × 10 min), membranes were incubated with HRP-conjugated secondary antibodies (1:5000, Cat# SA00001-1 for mouse, Cat# SA00001-2 for rabbit, Proteintech) for 1 h at room temperature. Protein bands were visualized using ECL reagent (Cat# A2581, ApexBio, Shanghai, China) and imaged with ChemiDoc™ XRS+ system (Cat# 1708265, Bio-Rad). Band intensities were quantified using ImageJ software (version 1.54f, NIH, Bethesda, MD, USA) and normalized to β-actin.

Cell Proliferation Assay

Cell proliferation was assessed using the Cell Counting Kit-8 (CCK-8; Cat# CK04, Lot# QR345, Dojindo Molecular Technologies, Kumamoto, Japan). Cells were seeded in 96-well plates at a density of 2000 cells per well. At designated time points (0, 24, 48, 72, and 96 hours), 10 µL of CCK-8 solution was added to each well and incubated for 2 hours at 37 °C. Absorbance was measured at 450 nm using a microplate reader (Synergy H1, Model SIAFRTD, BioTek Instruments, Winooski, VT, USA). Each experiment was performed in sextuplicate wells and repeated three times independently.

Transwell Migration and Invasion Assays

For migration assays, 5×10^4 cells in 200 µL serum-free medium were seeded into the upper chamber of Transwell inserts (8 µm pore size; Corning, NY), while the lower chamber contained 600 µL complete medium with 10% FBS as a chemoattractant. After 24 hours of incubation, non-migrated cells on the upper surface were removed with cotton swabs. Cells that migrated to the lower surface were fixed with 4% paraformaldehyde for 15 minutes, stained with 0.1% crystal violet for 20 minutes, and counted under a microscope in five random fields per insert.

For invasion assays, Transwell inserts were pre-coated with Matrigel (Cat# 356234, Lot# 3156789C, BD Biosciences, San Jose, CA, USA) diluted 1:8 in serum-free medium and incubated at 37 °C for 4 hours to allow gel formation. The procedure was otherwise identical to the migration assay, except that cells were incubated for 48 hours. All experiments were performed in triplicate and repeated three times independently.

Statistical Analysis

All statistical analyses were performed using R software (version 4.3.1) and GraphPad Prism (version 8.0.2, GraphPad Software, San Diego, CA, USA). Data are presented as mean ± standard deviation (SD) for normally distributed data, or as median with interquartile range (IQR) for non-normally distributed data. For single-cell and bulk tissue analyses: • Comparison of two groups: Wilcoxon signed-rank tests were used for paired data (e.g., TCGA paired tumor vs. normal samples) and Wilcoxon rank-sum tests for unpaired data (e.g., CPTAC protein expression, TCGA unpaired samples). • Multiple group comparisons: Kruskal-Wallis test followed by Dunn's post-hoc test with Bonferroni correction was employed for non-normally distributed data (e.g., *SRSF1* expression across different cell types). For *in vitro* experiments: • RT-qPCR, Western blot quantification, and functional assays (CCK-8, Transwell): One-way ANOVA followed by Tukey's post-hoc test was used to compare three groups (NC, sh-NC, sh-*SRSF1*) after confirming normal distribution using the Shapiro-Wilk test and homogeneity of variance using Levene's test. • Specific pairwise comparisons: sh-*SRSF1* vs. NC and sh-*SRSF1* vs. sh-NC. Correlation analyses: • Pearson correlation coefficient: Used for TCGA-UCEC bulk mRNA expression data, specifically for correlations between *SRSF1* and efferocytosis- related genes (*MERTK*, *AXL*, *TYRO3*, *GAS6*), assuming linear relationships and normally distributed continuous variables. • Spearman rank correlation coefficient: Used for single-cell RNA sequencing data due to non-normal distributions and potential outliers inherent to sparse single-cell expression profiles. All *p*-values are two-sided, with a $p < 0.05$ considered statistically significant (*$p < 0.05$, **$p < 0.01$, ***$p < 0.001$). Each *in vitro* experiment was independently conducted at least three times (n = 3 biological replicates), with technical replicates as specified: sextuplicate wells for CCK-8 assays, triplicate inserts for Transwell assays, and triplicate reactions for RT-qPCR.

Results

SRSF1 Is Upregulated in Endometrial Carcinoma at Both mRNA and Protein Levels

To establish the clinical relevance of *SRSF1* in endometrial carcinoma, we first analyzed its expression in bulk tissue datasets. Pan-cancer analysis across 33 cancer types using TCGA data revealed that *SRSF1* expression showed significant differences in 17 cancer types compared to their respective normal tissues, with 15 upregulated and 2 downregulated (Fig. 1A, $p < 0.05$).

Focusing specifically on endometrial carcinoma (UCEC), analysis of CPTAC proteomic data demonstrated significantly elevated *SRSF1* protein expression in tumor tissues compared to normal endometrium (Fig. 1B, $p < 0.05$). At the mRNA level, TCGA data analysis revealed that *SRSF1* expression was significantly higher in UCEC tumor tissues compared to normal tissues (Fig. 1C, $p < 0.05$). This finding was further validated in matched-paired samples, where *SRSF1* was consistently upregulated in tumor tissues compared to their paired normal counterparts (Fig. 1D, $p < 0.05$). To evaluate the diagnostic potential of *SRSF1*, we performed receiver operating characteristic (ROC) curve analysis, which yielded an area under the curve (AUC) of 0.702 (95% CI: 0.638–0.767) (Fig. 1E), suggesting moderate diagnostic value for distinguishing tumor from normal endometrial tissue.

Single-Cell Transcriptomic Landscape of the Endometrial Carcinoma Microenvironment

To comprehensively characterize the cellular composition and *SRSF1* expression patterns within the endometrial carcinoma microenvironment at single-cell resolution, we analyzed scRNA-seq data from five UCEC samples [28], comprising 35,868 cells initially. After applying stringent quality control criteria, a total of 33,178 high-quality cells were retained for downstream analysis.

Quality control metrics, including the number of detected genes (nFeature_RNA), total RNA counts (nCount_RNA), and percentage of mitochondrial genes (percent.MT), showed consistent patterns across the five tumor samples, with sample-specific variations reflecting biological heterogeneity (**Supplementary Fig. 1A**). Correlation analysis between quality control parameters revealed expected relationships: total RNA count was negatively correlated with mitochondrial gene percentage (r = –0.17), suggesting that cells with higher mitochondrial content tend to be of lower quality, and strongly positively correlated with the number of detected genes (r = 0.9), indicating robust quality of data (**Supplementary Fig. 1B**).

Identification of highly variable genes revealed key inflammatory mediators and chemokines, including *CCL3*, *CCL21*, *IGHG1*, and *IL1B*, which contribute significantly to cellular heterogeneity in the tumor microenvironment (Fig. 2D). Using unsupervised clustering based on global gene expression profiles, we identified 26 distinct cell clusters (clusters 0–25) (Fig. 2A). Through systematic annotation using established marker genes (Fig. 2C), these clusters were categorized into multiple cell types. The major stromal and immune components included Fibroblasts, Mesenchymal stem cells, Endothelial cells, T

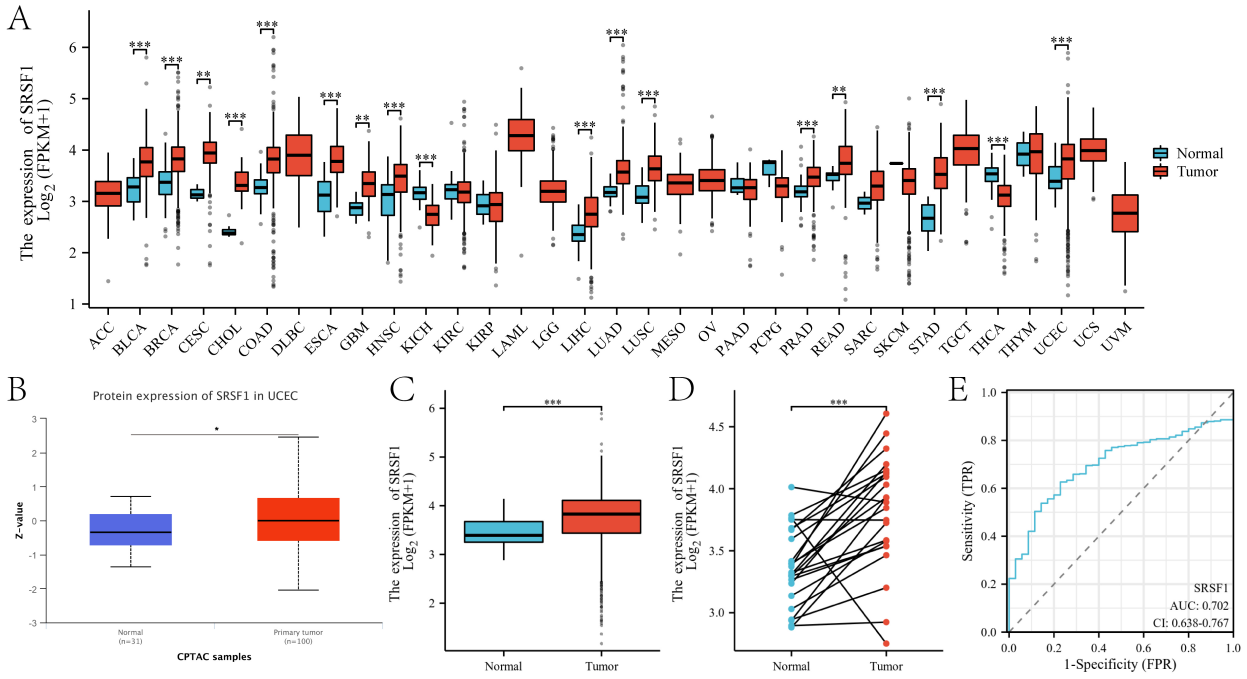

Fig. 1. Pan-cancer *SRSF1* expression and endometrial carcinoma validation. (A) Pan-cancer analysis of *SRSF1* mRNA expression (TCGA). (B) *SRSF1* expression in UCEC tumors vs. normal endometrium. (C) Paired sample analysis (TCGA). (D) Protein expression validation (CPTAC). (E) ROC curve analysis. $*p < 0.05$, $**p < 0.01$, $***p < 0.001$. *SRSF1*, Serine/arginine-rich splicing factor 1; UCEC, endometrial carcinoma; ROC, receiver operating characteristic.

Cells, Macrophages, Smooth muscle cells, and Mast Cells (Fig. 2B). Tumor epithelial cells were also identified and analyzed separately. The marker gene expression patterns for each cell type are shown in Fig. 2C, where dot size represents the percentage of cells expressing each marker and color intensity indicates average expression level.

SRSF1 Expression Patterns and Association With Efferocytosis Activity Across Cell Types

To investigate the expression pattern of *SRSF1* in the endometrial carcinoma microenvironment, its expression across all identified cell types was examined. Dot plot analysis revealed that *SRSF1* expression was significantly elevated in macrophages compared to other cell populations (Kruskal-Wallis test, $p < 0.05$) (Fig. 3A). Notably, *SRSF1* was also expressed at moderate levels in tumor epithelial cells, fibroblasts, and T cells, suggesting potential functional roles across multiple cell types within the tumor microenvironment.

Given the high expression of *SRSF1* in macrophages, we hypothesized that it might be associated with macrophage efferocytosis—the clearance of apoptotic cells—a critical function in tissue homeostasis and immune regulation [16,19,37]. To test this hypothesis, efferocytosis activity scores were calculated for all cells using a curated gene signature comprising receptors, bridging molecules, and signaling components involved in apoptotic cell recognition and engulfment.

UMAP visualization of efferocytosis score distribution demonstrated that macrophages displayed the highest efferocytosis activity, as evidenced by intense red-orange coloring, followed by fibroblasts and MSCs with intermediate activity (Fig. 3B). Histogram analysis of efferocytosis scores revealed that the majority of cells (25,841 out of 33,178) exhibited scores above the threshold of 0.073, indicating substantial efferocytosis-related transcriptional activity across the tumor microenvironment (Fig. 3C).

Venn diagram analysis revealed that, among the cell type marker genes, 137 genes overlapped with the efferocytosis gene signature, suggesting functional connections between cell identity and efferocytosis capacity (Fig. 3D). UMAP visualization of *SRSF1* spatial distribution confirmed its predominant expression in macrophage clusters, with additional expression detected in scattered tumor epithelial cells (Fig. 3E). This distinctive expression pattern, combined with the strong spatial overlap between regions of high *SRSF1* expression and elevated efferocytosis activity, suggests that *SRSF1* may play important roles in regulating macrophage function, potentially through modulation of alternative splicing programs [5,6].

SRSF1 Expression Correlates With Key Efferocytosis Receptors

To provide molecular evidence for the association between *SRSF1* and efferocytosis, correlations between *SRSF1* and key efferocytosis receptors were examined us-

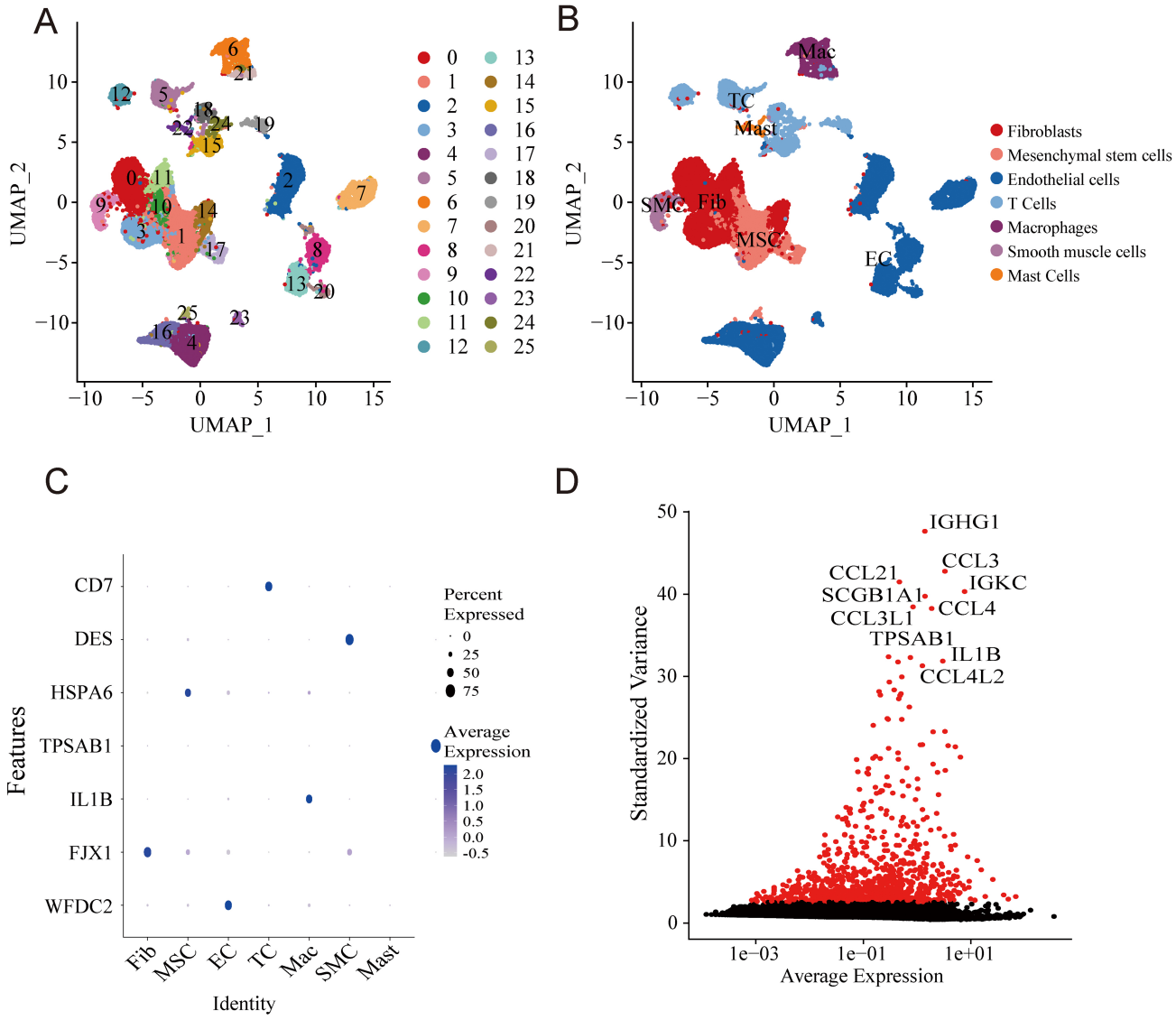

Fig. 2. Single-cell transcriptomic landscape of endometrial carcinoma microenvironment. (A) Uniform Manifold Approximation and Projection (UMAP) visualization of 26 cell clusters (numbers 0–25 represent individual clusters identified by unsupervised clustering). (B) Annotated major cell populations. (C) Cell type-specific marker expression. (D) Highly variable gene identification. Abbreviations: Mac, Macrophages; TC, T Cells; Mast, Mast Cells; SMC, Smooth Muscle Cells; Fib, Fibroblasts; MSC, Mesenchymal Stem Cells; EC, Endothelial Cells.

ing TCGA endometrial carcinoma data. Pearson correlation analysis revealed significant positive correlations (**Supplementary Fig. 2**): *SRSF1-MERTK*: R = 0.50, *SRSF1-AXL*: R = 0.42, *SRSF1-GAS6*: R = 0.54, *SRSF1-TYRO3*: R = 0.22, all $p < 0.001$. The strongest correlation with *GAS6* (R = 0.54), the principal ligand for TAM receptors, suggests coordinated regulation of the efferocytosis signaling axis. These correlations provide direct molecular evidence supporting functional relationships between *SRSF1* and efferocytosis machinery, extending beyond spatial co-localization patterns observed in single-cell analysis.

Correlation analyses between *SRSF1* and efferocytosis receptors are presented in **Supplementary Fig. 2**.

Functional Characteristics of Efferocytosis-Related Genes

To gain mechanistic insights into efferocytosis in the tumor microenvironment, we performed comprehensive functional enrichment analysis on efferocytosis-related genes. KEGG pathway analysis revealed significant enrichment in key immune-related pathways, including antigen processing and presentation, the IL-17 signaling pathway, Th17 cell differentiation, and NF-κB signaling (Fig. 3F).

Gene Ontology (GO) analysis of Biological Processes revealed significant enrichment in immune and inflammatory responses, antigen processing and presentation via MHC class II, neutrophil chemotaxis, positive regulation of cell migration, negative regulation of apoptotic processes,

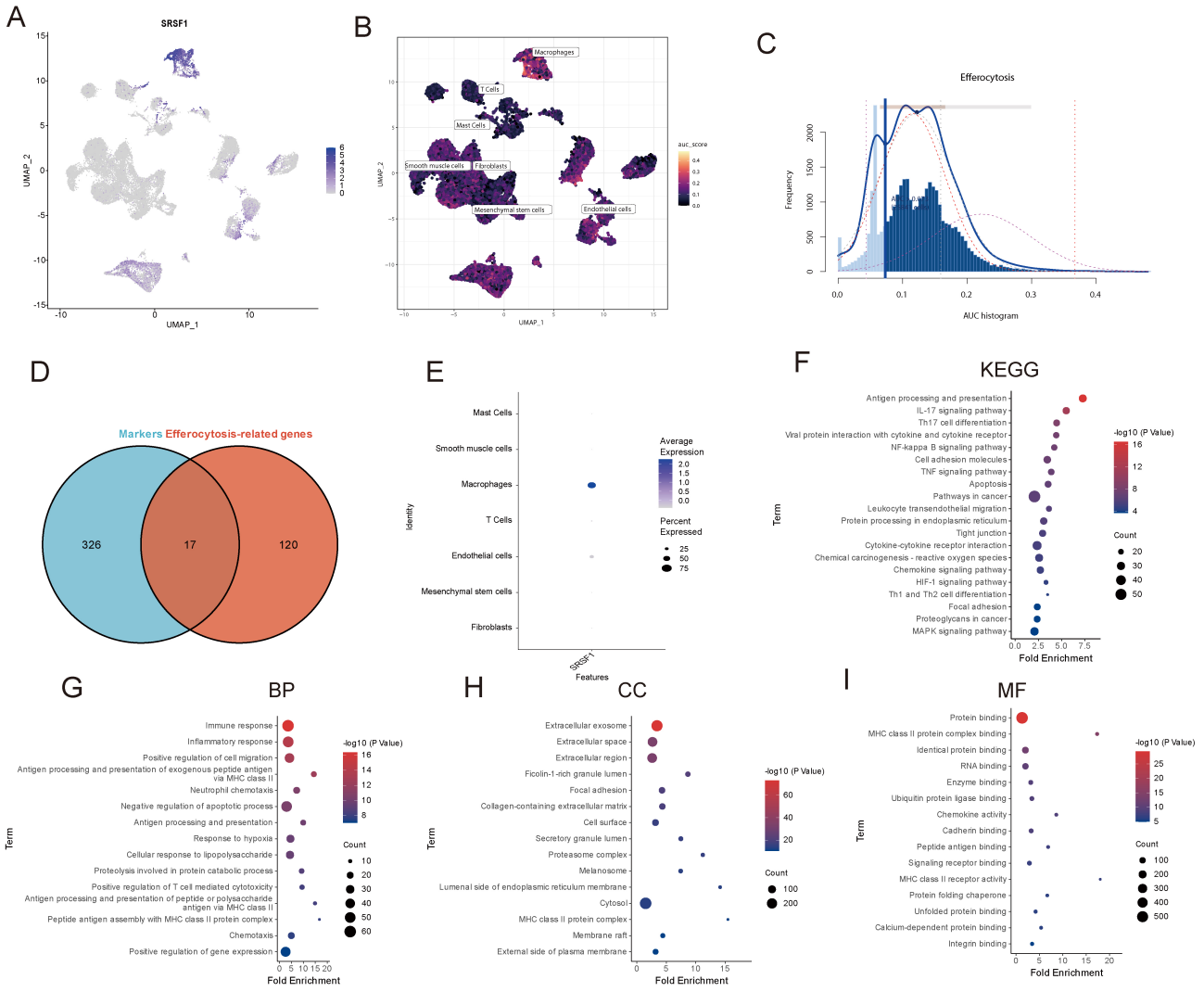

Fig. 3. *SRSF1* expression and efferocytosis activity across cell types. (A) *SRSF1* expression across cell types. (B) Efferocytosis activity distribution by UMAP. (C) Efferocytosis score histogram. (D) Overlap between marker genes and efferocytosis genes. (E) *SRSF1* spatial distribution. (F) KEGG pathway enrichment. (G) GO Biological Process enrichment. (H) GO Cellular Component enrichment. (I) GO Molecular Function enrichment. KEGG, Kyoto Encyclopedia of Genes and Genomes; GO, Gene Ontology.

and cellular response to lipopolysaccharide (Fig. 3G). Cellular Component analysis demonstrated prominent enrichment in extracellular exosomes, extracellular regions, and extracellular spaces (Fig. 3H). Molecular Function enrichment analysis highlighted a significant over-representation of protein binding functions, particularly MHC class II protein complex binding (Fig. 3I). These findings collectively indicate that efferocytosis-related genes in the tumor microenvironment participate in diverse immune regulatory processes.

Macrophage Heterogeneity and Pseudotime Trajectory Analysis

To better understand macrophage functional diversity in the endometrial carcinoma microenvironment, detailed subpopulation analysis of all macrophage cells was performed. Based on differential gene expression profiles, we identified seven distinct macrophage subgroups, each characterized by specific marker genes: *SDS*+ macrophages, *MMP9*+ macrophages, *CCL4L2*+ macrophages, *HSPA6*+ macrophages, *DAPP1*+ macrophages, *SERPINB2*+ macrophages, and *DCN*+ macrophages. Heatmap visualization revealed the unique expression patterns of these marker genes across the seven subgroups (Fig. 4A).

To explore macrophage differentiation trajectories, pseudotime analysis was performed using Monocle 2. The resulting trajectory topology revealed a branched structure, indicating that macrophages differentiate along multiple distinct paths within the tumor microenvironment (Fig. 4B). Analysis of cell distribution along the pseudotime trajectory showed distinct positioning of different macrophage subpopulations (Fig. 4C), while the branch trajectory diagram

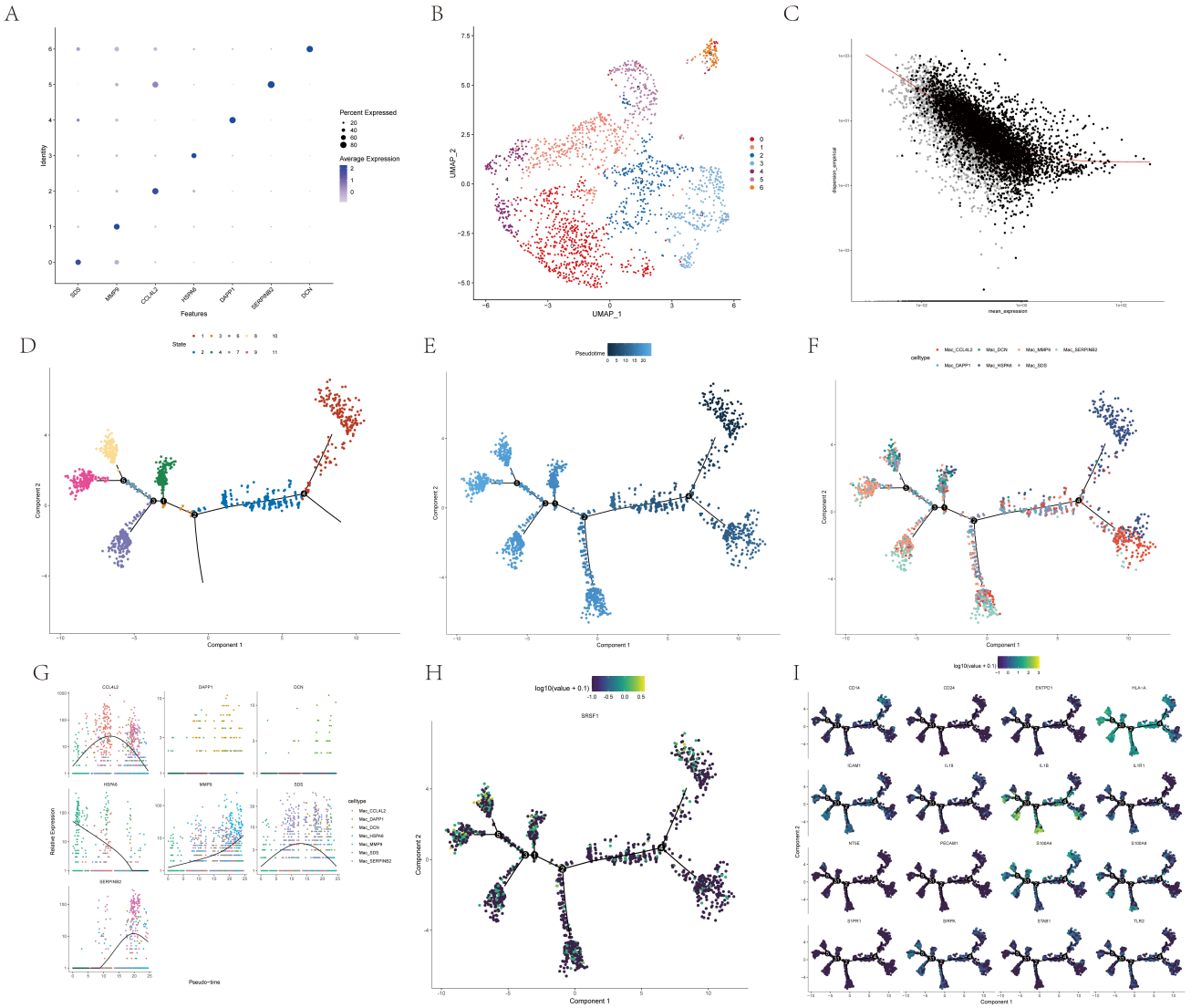

Fig. 4. Macrophage heterogeneity and pseudotime trajectory analysis. (A) Heatmap of macrophage subgroup markers. The vertical axis represents seven macrophage subgroups: *SDS*+, *MMP9*+, *CCL4L2*+, *HSPA6*+, *DAPP1*+, *SERPINB2*+, and *DCN*+ macrophages. (B) Pseudotime trajectory topology. (C) Cell distribution along the trajectory. (D) Branch trajectory diagram. (E) Cell density distribution. (F) Cell state distribution. (G) Marker gene expression dynamics. (H) *SRSF1* expression along the trajectory. (I) Spatial distribution of functionally significant genes.

further illustrated key bifurcation points in macrophage differentiation (Fig. 4D). Cell density distribution analysis revealed regions of high cell concentration along specific trajectory branches (Fig. 4E), while cell state distribution mapping identified discrete functional states corresponding to different positions along the pseudotime continuum (Fig. 4F).

Analysis of marker gene expression dynamics along the pseudotime trajectory revealed that the seven macrophage subtype marker genes exhibited unique expression patterns at specific cellular states or transition points (Fig. 4G). Notably, *SRSF1* expression showed dynamic changes along the pseudotime trajectory, with varying levels across different macrophage states and differentiation branches (Fig. 4H). Spatial distribution analysis of functionally significant genes further revealed coordinate expression patterns that may underlie macrophage functional specialization (Fig. 4I).

Cell-Cell Communication Networks in the Tumor Microenvironment

To understand how macrophages interact with other cell types in the endometrial carcinoma microenvironment, a comprehensive cell-cell communication analysis was performed using CellChat. This analysis revealed extensive communication networks between macrophages and various other cell populations, with circular plots illustrating the complexity and intensity of these interactions (Fig. 5A).

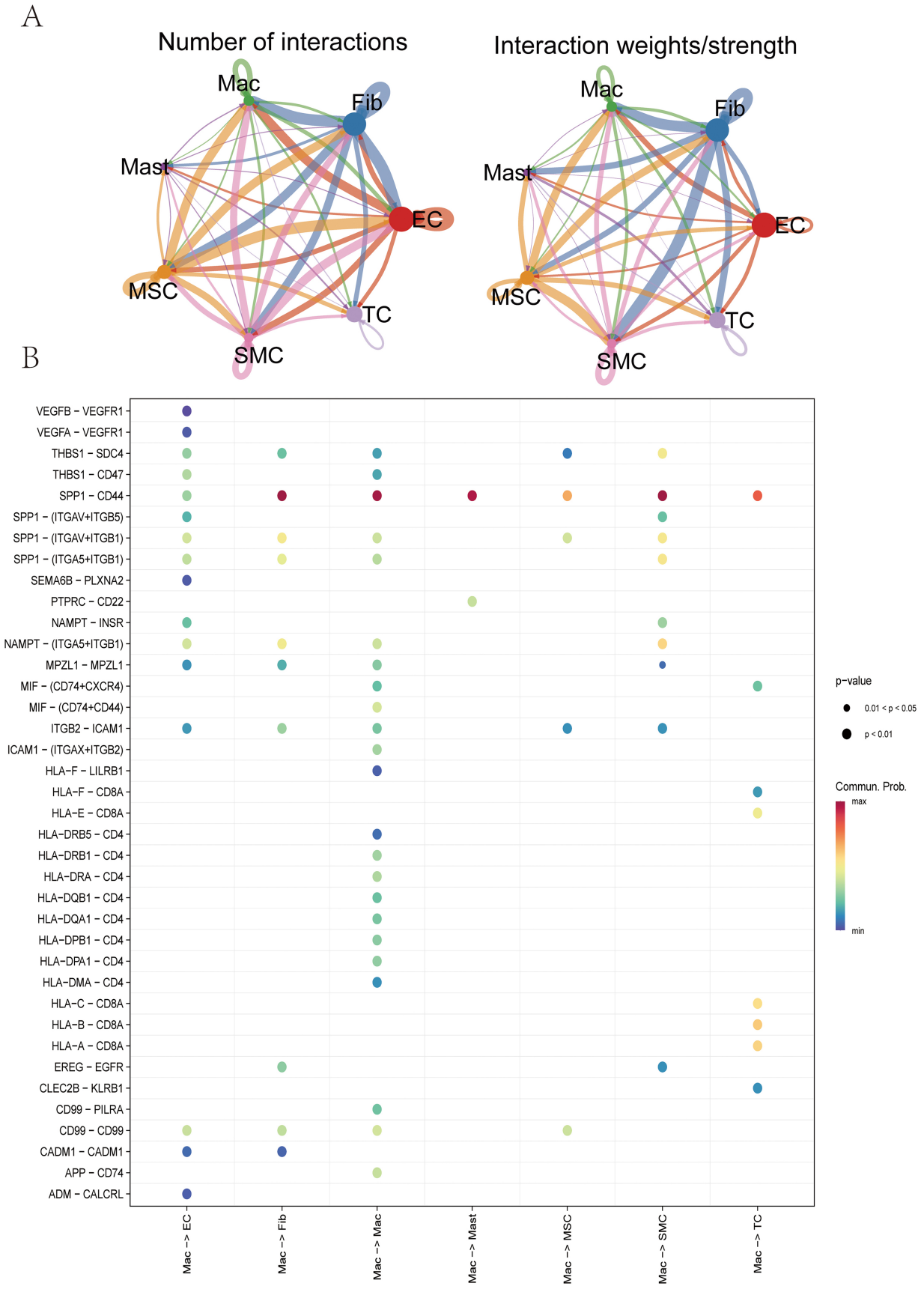

Fig. 5. Cell-cell communication networks in the tumor microenvironment. (A) Macrophage-centered communication networks. (B) Ligand-receptor interaction heatmap.

Macrophages showed particularly strong signaling interactions with tumor epithelial cells, fibroblasts, and T cells, suggesting their central role in orchestrating communication within the tumor microenvironment.

Detailed examination of specific ligand-receptor pairs revealed several critical signaling pathways mediating these interactions (Fig. 5B). Heatmap visualization showed the relative contribution of different ligand-receptor pairs to cell-cell communication, with the *SPP1-CD44* signaling axis emerging as particularly prominent. Other important interaction pairs included those involved in growth factor signaling, cytokine-receptor binding, and cell adhesion molecules. These findings highlight the intricate communication networks through which macrophages influence and are influenced by other cell types in the tumor microenvironment.

SRSF1 Knockdown Inhibits Endometrial Cancer Cell Proliferation, Migration, and Invasion

Given the expression of *SRSF1* in tumor epithelial cells observed in our single-cell analysis and its established role in cancer progression, we investigated the functional impact of *SRSF1* on endometrial cancer cell behavior using the Ishikawa cell line, a well-characterized Type I endometrioid adenocarcinoma model that represents the most common histological subtype of endometrial cancer.

Three experimental groups were established using lentiviral-mediated shRNA delivery: NC (blank control without lentiviral transduction), sh-NC (scrambled shRNA control), and sh-*SRSF1* (*SRSF1*-targeted shRNA). RT-qPCR analysis confirmed effective knockdown of *SRSF1* mRNA in the sh-*SRSF1* group, with knockdown efficiency of approximately 70% compared to both NC and sh-NC controls (Fig. 6A, $***p < 0.001$).

To assess the impact of *SRSF1* on cell proliferation, we performed CCK-8 assays over a 96-hour time course across all three groups. *SRSF1* knockdown (sh-*SRSF1*) significantly suppressed Ishikawa cell proliferation compared to both NC and sh-NC control groups (Fig. 6B). The growth inhibition was most pronounced at 72 and 96 hours, with reductions of approximately 30–40% in cell viability in the sh-*SRSF1* group compared to controls ($p < 0.05$). Transwell migration and Matrigel invasion assays were performed to evaluate the effects of *SRSF1* on cell motility and invasive capacity across the three groups. Representative microscopic images showed a marked reduction in the number of migrated and invaded cells in the sh-*SRSF1* group compared to NC and sh-NC controls (Fig. 6D). Quantitative analysis demonstrated that *SRSF1* knockdown significantly reduced the number of migrated cells by approximately 50% and invaded cells by approximately 50–60% compared to control groups (Fig. 6C, $p < 0.05$). Western blot analysis confirmed the reduction of *SRSF1* protein levels in the sh-*SRSF1* group compared to NC and sh-NC controls (Fig. 6E). To investigate whether *SRSF1*'s effects on migration and invasion involve modulation of epithelial-mesenchymal transition (EMT), the expression of key EMT markers was examined using Western blot across all three groups. *SRSF1* knockdown resulted in increased expression of E-cadherin (an epithelial marker) and decreased expression of N-cadherin and vimentin (mesenchymal markers) in Ishikawa cells (Fig. 6F), consistent with a reversal of EMT. These results demonstrate that *SRSF1* promotes endometrial cancer cell proliferation, migration, invasion, and EMT, highlighting its oncogenic role in tumor cell-intrinsic mechanisms.

Discussion

This study provides the first comprehensive single-cell analysis of *SRSF1* expression in the endometrial carcinoma microenvironment, revealing its preferential expression in tumor-associated macrophages and strong spatial association with efferocytosis activity, suggesting that *SRSF1* plays multifaceted roles in endometrial carcinoma progression through both tumor cell-intrinsic mechanisms and modulation of the tumor immune microenvironment. Our single-cell analysis revealed that *SRSF1* expression is significantly elevated in tumor-associated macrophages compared to other cell types, a cell-type-specific expression pattern that has not been previously reported, and suggests that *SRSF1* may have particularly important functions in regulating macrophage biology within the tumor context. While *SRSF1*'s roles in tumor cells have been extensively explored [7–11], its functions in immune cells, particularly macrophages, remain largely unexplored. The preferential expression of *SRSF1* in macrophages is notable, given the well-established roles of alternative splicing in regulating immune cell function and activation states [37]. Macrophages exhibit remarkable plasticity, transitioning between pro-inflammatory (M1-like) and anti-inflammatory/immunosuppressive (M2-like) phenotypes in response to microenvironmental cues [14,15]. Our pseudotime analysis revealed seven functionally distinct macrophage subpopulations with varying *SRSF1* expression levels, suggesting that *SRSF1* may participate in regulating macrophage differentiation and polarization. One of the most striking findings is the strong spatial overlap between regions of high *SRSF1* expression and elevated efferocytosis activity, particularly within macrophage populations [16,37], which is notable given that efferocytosis plays complex and context-dependent roles in tumor biology [19–21]. Our functional enrichment analysis of efferocytosis-related genes revealed significant involvement in immune responses, antigen processing and presentation, and immunomodulatory signaling pathways, including IL-17 and NF-κB. Our correlation analysis provides mechanistic insights into how *SRSF1* may regulate macrophage efferocytosis. The significant correlations with *MERTK*, *AXL* and particularly *GAS6* suggest *SRSF1*

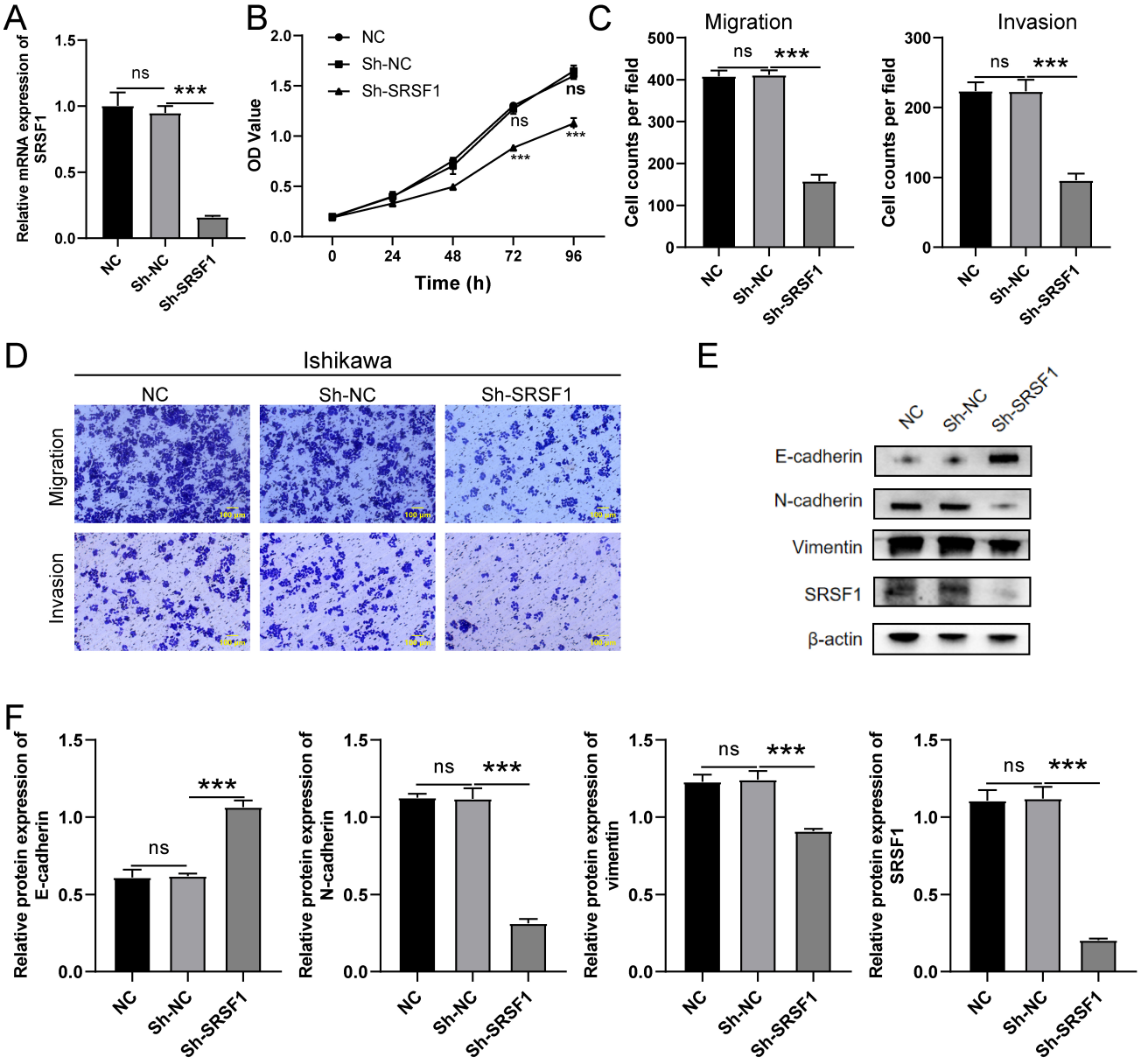

Fig. 6. *SRSF1* functional validation in Ishikawa endometrial cancer cells (n = 3 independent experiments). (A) *SRSF1* knockdown efficiency validation by RT-qPCR. (B) Cell proliferation assays (CCK-8) showing time-dependent growth inhibition. (C) Quantification of migrated and invaded cells. (D) Representative images of Transwell migration and invasion assays. (E) Western blot validation of *SRSF1* protein knockdown. (F) Epithelial-mesenchymal transition (EMT) marker expression analysis showing E-cadherin upregulation and N-cadherin/vimentin downregulation upon *SRSF1* knockdown.*** $p < 0.001$, ns, not significant.

may control efferocytosis through alternative splicing of TAM receptors. Previous studies demonstrate that *MERTK* undergoes alternative splicing to generate soluble forms that inhibit efferocytosis signaling [38,39], and *SRSF1* may regulate this balance between functional isoforms. The strong *SRSF1-GAS6* correlation suggests potential transcriptional co-regulation, as *GAS6* bridges apoptotic cells to phagocyte receptors. Our pseudotime analysis showing dynamic *SRSF1* expression along macrophage differentiation trajectories suggests *SRSF1* participates in macrophage functional state transitions. The varying *SRSF1* levels across seven macrophage subpopulations indicate cell state-specific expression, with high-*SRSF1* macrophages potentially specialized for efferocytosis. Additionally, our CellChat analysis identified the *SPP1-CD44* axis as prominent in macrophage communication. Since *SRSF1* regulates *CD44* alternative splicing [40], it may modulate macrophage interactions by controlling *CD44* isoform expression, affecting both cell adhesion and activation states. These observations position this study as an exploratory,

proof-of-concept investigation supporting *SRSF1*'s role in regulating the tumor microenvironment. While we have not performed mechanistic validation in macrophages, the convergent evidence from spatial analysis, correlation data, and trajectory dynamics establishes a foundation for future mechanistic investigations. The correlation data particularly provide specific testable hypotheses regarding *SRSF1*-regulated splicing events in efferocytosis receptors. As a master regulator of alternative splicing, *SRSF1* could modulate the expression or function of key efferocytosis receptors (such as *MERTK*, *AXL*, and *CD36*), bridging molecules (such as *GAS6* and MFG-E8), and downstream signaling components through control of splice isoform selection [5, 6]. Notably, many efferocytosis-related genes undergo alternative splicing, generating protein isoforms with distinct functional properties, as exemplified by different splice variants of *MERTK* that differentially regulate macrophage activation states [38,39]. Our cell-cell communication analysis revealed that macrophages engage in extensive bidirectional signaling with multiple cell types in the tumor microenvironment, particularly tumor epithelial cells and fibroblasts, with the prominence of the *SPP1-CD44* signaling axis being noteworthy, as this pathway has been implicated in promoting tumor cell survival, invasion, and therapy resistance [41]. *SRSF1* has been shown to regulate alternative splicing of *CD44*, generating different isoforms with distinct signaling properties [40]. Our functional validation experiments in the Ishikawa endometrial cancer cell line demonstrated that *SRSF1* directly promotes tumor cell proliferation, migration, invasion, and EMT, which is consistent with previous studies in other cancer types showing that *SRSF1* functions as an oncogenic splicing factor [7–11]. Ishikawa cell line, derived from a well-differentiated Type I endometrioid adenocarcinoma, represents an appropriate model for studying *SRSF1* function in the most common histological subtype of endometrial cancer [42,43]. Importantly, our observation that *SRSF1* modulates EMT markers in Ishikawa cells suggests it may regulate splicing of EMT-related transcription factors or signaling molecules, and the consistency of *SRSF1*'s tumor-promoting functions in this well-characterized endometrial cancer cell line supports its potential as a therapeutic target in endometrial carcinoma. Our findings have several potential clinical implications, as the upregulation of *SRSF1* in endometrial carcinoma at both mRNA and protein levels suggests it could serve as a biomarker for disease diagnosis or prognosis, and more importantly, *SRSF1* represents an attractive therapeutic target due to its dual roles in tumor cells and the microenvironment. Several strategies for targeting splicing factors are under development, including antisense oligonucleotides and small molecule inhibitors [44,45], and recent work has demonstrated that targeting *SRSF1* can enhance cancer immunotherapy efficacy [16], which, given the recent approval of immune checkpoint inhibitors for advanced endometrial cancer [46], suggests that exploring combinations with splicing-targeted therapies could improve patient outcomes. Recent studies have highlighted the critical role of macrophage-associated immune markers in predicting immunotherapy response across multiple cancer types, and the PD-L1 macrophage score has emerged as a potential predictive biomarker in gastrointestinal cancers [47,48]. Given our finding of preferential *SRSF1* expression in tumor-associated macrophages, future studies should investigate whether *SRSF1* expression correlates with PD-L1 status in macrophages and whether this relationship influences immunotherapy efficacy in endometrial carcinoma. Several limitations should be acknowledged. First, while our correlation analysis provides molecular evidence linking *SRSF1* to efferocytosis receptors, functional experiments in macrophages are needed to establish causality. Future studies should investigate *SRSF1* function in macrophages through knockdown or overexpression experiments, assess efferocytosis activity using functional assays, and identify specific splicing events of TAM receptors regulated by *SRSF1*. Second, our functional validation was limited to the Ishikawa cell line; additional endometrial cancer cell lines, patient-derived organoids, and *in vivo* models require comprehensive validation. Third, we analyzed only the GSE173682 dataset (n = 5 samples); validation in additional cohorts and spatial transcriptomics would strengthen generalizability. Fourth, correlations do not establish causation—CRISPR-based knockout and rescue experiments are necessary to confirm direct regulatory relationships. Finally, we did not correlate *SRSF1* expression with clinical outcomes; future studies should assess its prognostic value and association with treatment response. Despite these limitations, this study offers several unique contributions: (1) the first single-cell characterization of *SRSF1* in endometrial carcinoma, revealing its preferential TAM expression; (2) molecular evidence linking *SRSF1* to efferocytosis machinery; (3) a comprehensive analysis of macrophage heterogeneity; (4) multi-modal validation combining bioinformatics with experiments; and (5) proof-of-concept that *SRSF1* represents a dual target affecting tumor cells and microenvironment. These findings provide a foundation for the mechanistic studies outlined above.

Conclusion

This exploratory study provides the first comprehensive single-cell characterization of *SRSF1* expression in the endometrial carcinoma microenvironment. We demonstrate that *SRSF1* is preferentially expressed in tumor-associated macrophages and shows a strong spatial correlation with efferocytosis activity. Correlation analysis revealed significant associations between *SRSF1* and key efferocytosis receptors (*MERTK*, *AXL*, *GAS6*), providing molecular evidence for functional relationships. Additionally, functional validation in the Ishikawa endometrial cancer cell line confirmed that *SRSF1* promotes malignant phe-

notypes, including proliferation, migration, invasion, and EMT. Our findings suggest that *SRSF1* may function as a central regulator connecting tumor cell-intrinsic oncogenic mechanisms with microenvironmental factors, positioning it as an attractive target for therapeutic intervention. While definitive mechanistic validation in macrophages remains to be addressed in future studies, this work provides critical proof-of-concept evidence and generates specific, testable hypotheses regarding *SRSF1*-mediated regulation of macrophage efferocytosis through alternative splicing mechanisms. These results establish a foundation for future mechanistic studies that may ultimately inform novel *SRSF1*-targeted diagnostic and therapeutic strategies for endometrial carcinoma.

Availability of Data and Materials

The single-cell RNA sequencing data analyzed in this study are publicly available in the Gene Expression Omnibus (GEO) database under accession number GSE173682. Bulk tissue transcriptomic data were obtained from The Cancer Genome Atlas (TCGA) database (https://portal.gdc.cancer.gov/) and proteomic data from the Clinical Proteomic Tumor Analysis Consortium (CPTAC) database (https://proteomics.cancer.gov/programs/cptac). Additional data generated from the GEPIA platform (http://gepia.cancer-pku.cn/) are also publicly accessible. All other data supporting the findings of this study are available from the corresponding author upon reasonable request.

Author Contributions

AZ: Conceptualization, Data curation, Formal analysis, Investigation, Methodology, Visualization, Writing - original draft, Writing - review & editing. YG: Data curation, Formal analysis, Validation, Visualization, Writing - review & editing. RF: Data curation, Formal analysis, Writing - review & editing. ZL: Data curation, Formal analysis, Writing - review & editing. QZ: Conceptualization, Funding acquisition, Project administration, Resources, Supervision, Writing - review & editing. All authors have read and approved the final manuscript. All authors have participated sufficiently in the work to take public responsibility for appropriate portions of the content and agreed to be accountable for all aspects of the work in ensuring that questions related to its accuracy or integrity.

Ethics Approval and Consent to Participate

This study utilized publicly available de-identified datasets from TCGA, CPTAC, and GEO databases. All original data were collected with appropriate ethics approval and informed consent as described in the original publications. For the *in vitro* experimental component using the Ishikawa cell line, no human subjects or animal experiments were involved, and therefore ethics approval was not required. The study was conducted in accordance with the Declaration of Helsinki and relevant institutional guidelines.

Acknowledgment

We thank the researchers who generated and shared the publicly available datasets used in this study, including the TCGA Research Network, the Clinical Proteomic Tumor Analysis Consortium (CPTAC), and the contributors of the GSE173682 dataset. We also acknowledge the use of computational resources and bioinformatics tools that facilitated this analysis.

Funding

This study is supported by Key scientific research project of the Anhui Provincial Department of Education (2024AH051247) and Key Scientific Research Projects via "Open Bidding for Champions" of Bengbu Medical University (2025byjbgs026).

Conflict of Interest

The authors declare no conflict of interest.

Supplementary Material

Supplementary material associated with this article can be found, in the online version, at https://doi.org/10.24976/Discov.Med.202638207.93.

References

[1] Sung H, Ferlay J, Siegel RL, Laversanne M, Soerjomataram I, Jemal A, *et al*. Global Cancer Statistics 2020: GLOBOCAN Estimates of Incidence and Mortality Worldwide for 36 Cancers in 185 Countries. CA: A Cancer Journal for Clinicians. 2021; 71: 209–249. https://doi.org/10.3322/caac.21660.

[2] Crosbie EJ, Kitson SJ, McAlpine JN, Mukhopadhyay A, Powell ME, Singh N. Endometrial cancer. Lancet (London, England). 2022; 399: 1412–1428. https://doi.org/10.1016/S0140-6736(22)00323-3.

[3] Morice P, Leary A, Creutzberg C, Abu-Rustum N, Darai E. Endometrial cancer. Lancet (London, England). 2016; 387: 1094–1108. https://doi.org/10.1016/S0140-6736(15)00130-0.

[4] Lu KH, Broaddus RR. Endometrial Cancer. The New England Journal of Medicine. 2020; 383: 2053–2064. https://doi.org/10.1056/NEJMra1514010.

[5] Chen M, Manley JL. Mechanisms of alternative splicing regulation: insights from molecular and genomics approaches. Nature Reviews. Molecular Cell Biology. 2009; 10: 741–754. https://doi.org/10.1038/nrm2777.

[6] Long JC, Caceres JF. The SR protein family of splicing factors: master regulators of gene expression. The Biochemical Journal. 2009; 417: 15–27. https://doi.org/10.1042/BJ20081501.

[7] Karni R, de Stanchina E, Lowe SW, Sinha R, Mu D, Krainer AR. The gene encoding the splicing factor SF2/ASF is a proto-

oncogene. Nature Structural & Molecular Biology. 2007; 14: 185–193. https://doi.org/10.1038/nsmb1209.

[8] Das S, Anczuków O, Akerman M, Krainer AR. Oncogenic splicing factor *SRSF1* is a critical transcriptional target of MYC. Cell Reports. 2012; 1: 110–117. https://doi.org/10.1016/j.celrep.2011.12.001.

[9] Anczuków O, Rosenberg AZ, Akerman M, Das S, Zhan L, Karni R, *et al*. The splicing factor *SRSF1* regulates apoptosis and proliferation to promote mammary epithelial cell transformation. Nature Structural & Molecular Biology. 2012; 19: 220–228. https://doi.org/10.1038/nsmb.2207.

[10] Karni R, Hippo Y, Lowe SW, Krainer AR. The splicing-factor oncoprotein SF2/ASF activates mTORC1. Proceedings of the National Academy of Sciences of the United States of America. 2008; 105: 15323–15327. https://doi.org/10.1073/pnas.0801376105.

[11] Gonçalves V, Pereira JFS, Jordan P. Signaling Pathways Driving Aberrant Splicing in Cancer Cells. Genes. 2017; 9: 9. https://doi.org/10.3390/genes9010009.

[12] Wu H, Sun S, Tu K, Gao Y, Xie B, Krainer AR, *et al*. A splicing-independent function of SF2/ASF in microRNA processing. Molecular Cell. 2010; 38: 67–77. https://doi.org/10.1016/j.molcel.2010.02.021.

[13] Hanahan D, Weinberg RA. Hallmarks of cancer: the next generation. Cell. 2011; 144: 646–674. https://doi.org/10.1016/j.cell.2011.02.013.

[14] Noy R, Pollard JW. Tumor-associated macrophages: from mechanisms to therapy. Immunity. 2014; 41: 49–61. https://doi.org/10.1016/j.immuni.2014.06.010.

[15] Lopez-Yrigoyen M, Cassetta L, Pollard JW. Macrophage targeting in cancer. Annals of the New York Academy of Sciences. 2021; 1499: 18–41. https://doi.org/10.1111/nyas.14377.

[16] Lu SX, De Neef E, Thomas JD, Sabio E, Rousseau B, Gigoux M, *et al*. Pharmacologic modulation of RNA splicing enhances anti-tumor immunity. Cell. 2021; 184: 4032–4047.e31. https://doi.org/10.1016/j.cell.2021.05.038.

[17] Savill J, Dransfield I, Gregory C, Haslett C. A blast from the past: clearance of apoptotic cells regulates immune responses. Nature Reviews. Immunology. 2002; 2: 965–975. https://doi.org/10.1038/nri957.

[18] Gregory CD, Pound JD. Cell death in the neighbourhood: direct microenvironmental effects of apoptosis in normal and neoplastic tissues. The Journal of Pathology. 2011; 223: 177–194. https://doi.org/10.1002/path.2792.

[19] Yin C, Heit B. Cellular Responses to the Efferocytosis of Apoptotic Cells. Frontiers in Immunology. 2021; 12: 631714. https://doi.org/10.3389/fimmu.2021.631714.

[20] Werfel TA, Elion DL, Rahman B, Hicks DJ, Sanchez V, Gonzales-Ericsson PI, *et al.* Treatment-Induced Tumor Cell Apoptosis and Secondary Necrosis Drive Tumor Progression in the Residual Tumor Microenvironment through MerTK and IDO1. Cancer Research. 2019; 79: 171–182. https://doi.org/10.1158/0008-5472.CAN-18-1106.

[21] Birge RB, Boeltz S, Kumar S, Carlson J, Wanderley J, Calianese D, *et al*. Phosphatidylserine is a global immunosuppressive signal in efferocytosis, infectious disease, and cancer. Cell Death and Differentiation. 2016; 23: 962–978. https://doi.org/10.1038/cdd.2016.11.

[22] Chen G, Ning B, Shi T. Single-Cell RNA-Seq Technologies and Related Computational Data Analysis. Frontiers in Genetics. 2019; 10: 317. https://doi.org/10.3389/fgene.2019.00317.

[23] Slavin I, Carissimo A, Panariello F, Grimaldi A, Bouché V, Gambardella G, *et al*. Single-Cell RNA-Seq Analysis: A Step-by-Step Overview. Methods in Molecular Biology. 2021; 2284: 343–365. https://doi.org/10.1007/978-1-0716-1307-8_19.

[24] Yu T, Cazares O, Tang AD, Kim HY, Wald T, Verma A, *et al*. *SRSF1* governs progenitor-specific alternative splicing to maintain adult epithelial tissue homeostasis and renewal. Developmental Cell. 2022; 57: 624–637.e4. https://doi.org/10.1016/j.devcel.2022.01.011.

[25] Cancer Genome Atlas Research Network, Kandoth C, Schultz N, Cherniack AD, Akbani R, Liu Y, *et al*. Integrated genomic characterization of endometrial carcinoma. Nature. 2013; 497: 67–73. https://doi.org/10.1038/nature12113.

[26] Dou Y, Kawaler EA, Cui Zhou D, Gritsenko MA, Huang C, Blumenberg L, *et al*. Proteogenomic Characterization of Endometrial Carcinoma. Cell. 2020; 180: 729–748.e26. https://doi.org/10.1016/j.cell.2020.01.026.

[27] Robin X, Turck N, Hainard A, Tiberti N, Lisacek F, Sanchez JC, *et al*. pROC: an open-source package for R and S+ to analyze and compare ROC curves. BMC Bioinformatics. 2011; 12: 77. https://doi.org/10.1186/1471-2105-12-77.

[28] Regner MJ, Wisniewska K, Garcia-Recio S, Thennavan A, Mendez-Giraldez R, Malladi VS, *et al*. A multi-omic single-cell landscape of human gynecologic malignancies. Molecular Cell. 2021; 81: 4924–4941.e10. https://doi.org/10.1016/j.molcel.2021.10.013.

[29] Hao Y, Hao S, Andersen-Nissen E, Mauck WM, 3rd, Zheng S, Butler A, *et al*. Integrated analysis of multimodal single-cell data. Cell. 2021; 184: 3573–3587.e29. https://doi.org/10.1016/j.cell.2021.04.048.

[30] Wang W, Vilella F, Alama P, Moreno I, Mignardi M, Isakova A, *et al*. Single-cell transcriptomic atlas of the human endometrium during the menstrual cycle. Nature Medicine. 2020; 26: 1644–1653. https://doi.org/10.1038/s41591-020-1040-z.

[31] Garcia-Alonso L, Handfield LF, Roberts K, Nikolakopoulou K, Fernando RC, Gardner L, *et al*. Mapping the temporal and spatial dynamics of the human endometrium in vivo and in vitro. Nature Genetics. 2021; 53: 1698–1711. https://doi.org/10.1038/s41588-021-00972-2.

[32] Aibar S, González-Blas CB, Moerman T, Huynh-Thu VA, Imrichova H, Hulselmans G, *et al*. SCENIC: single-cell regulatory network inference and clustering. Nature Methods. 2017; 14: 1083–1086. https://doi.org/10.1038/nmeth.4463.

[33] Wu T, Hu E, Xu S, Chen M, Guo P, Dai Z, *et al*. clusterProfiler 4.0: A universal enrichment tool for interpreting omics data. Innovation (Cambridge (Mass.)). 2021; 2: 100141. https://doi.org/10.1016/j.xinn.2021.100141.

[34] Qiu X, Mao Q, Tang Y, Wang L, Chawla R, Pliner HA, *et al*. Reversed graph embedding resolves complex single-cell trajectories. Nature Methods. 2017; 14: 979–982. https://doi.org/10.1038/nmeth.4402.

[35] Trapnell C, Cacchiarelli D, Grimsby J, Pokharel P, Li S, Morse M, *et al*. The dynamics and regulators of cell fate decisions are revealed by pseudotemporal ordering of single cells. Nature Biotechnology. 2014; 32: 381–386. https://doi.org/10.1038/nbt.2859.

[36] Jin S, Guerrero-Juarez CF, Zhang L, Chang I, Ramos R, Kuan CH, *et al*. Inference and analysis of cell-cell communication using CellChat. Nature Communications. 2021; 12: 1088. https://doi.org/10.1038/s41467-021-21246-9.

[37] Paz S, Ritchie A, Mauer C, Caputi M. The RNA binding protein *SRSF1* is a master switch of gene expression and regulation in the immune system. Cytokine & Growth Factor Reviews. 2021; 57: 19–26. https://doi.org/10.1016/j.cytogfr.2020.10.008.

[38] Sather S, Kenyon KD, Lefkowitz JB, Liang X, Varnum BC, Henson PM, *et al*. A soluble form of the Mer receptor tyrosine kinase inhibits macrophage clearance of apoptotic cells and platelet aggregation. Blood. 2007; 109: 1026–1033. https://doi.org/10.1182/blood-2006-05-021634.

[39] Thorp E, Vaisar T, Subramanian M, Mautner L, Blobel C, Tabas I. Shedding of the Mer tyrosine kinase receptor is mediated by

ADAM17 protein through a pathway involving reactive oxygen species, protein kinase Cδ, and p38 mitogen-activated protein kinase (MAPK). Journal of Biological Chemistry. 2011; 286: 33335–33344. https://doi.org/10.1074/jbc.M111.263020.

[40] Prochazka L, Tesarik R, Turanek J. Regulation of alternative splicing of *CD44* in cancer. Cellular Signalling. 2014; 26: 2234–2239. https://doi.org/10.1016/j.cellsig.2014.07.011.

[41] Wai PY, Kuo PC. Osteopontin: regulation in tumor metastasis. Cancer Metastasis Reviews. 2008; 27: 103–118. https://doi.org/10.1007/s10555-007-9104-9.

[42] Nishida M. The Ishikawa cells from birth to the present. Human Cell. 2002; 15: 104–117. https://doi.org/10.1111/j.1749-0774.2002.tb00105.x.

[43] Holinka CF, Hata H, Kuramoto H, Gurpide E. Effects of steroid hormones and antisteroids on alkaline phosphatase activity in human endometrial cancer cells (Ishikawa line). Cancer Research. 1986; 46: 2771–2774.

[44] Bonnal SC, López-Oreja I, Valcárcel J. Roles and mechanisms of alternative splicing in cancer - implications for care. Nature Reviews. Clinical Oncology. 2020; 17: 457–474. https://doi.org/10.1038/s41571-020-0350-x.

[45] Anczuków O, Krainer AR. Splicing-factor alterations in cancers. RNA. 2016; 22: 1285–1301. https://doi.org/10.1261/rna.057919.116.

[46] Mirza MR, Chase DM, Slomovitz BM, dePont Christensen R, Novák Z, Black D, *et al*. Dostarlimab for Primary Advanced or Recurrent Endometrial Cancer. The New England Journal of Medicine. 2023; 388: 2145–2158. https://doi.org/10.1056/NEJMoa2216334.

[47] Rajpoot A, Sharma V. Bridging Cancer and Cardiovascular Health: A Comprehensive Review of Cardiotoxicity in Modern Oncology. Heart and Mind. 2025; 9: 115–135. https://doi.org/10.4103/hm.HM-D-24-00148.

[48] Baş Y. Is the “PD-L1 macrophage score” possible as an immunotherapy target in colon adenocarcinoma? Gastrointestinal Tumors. 2024; 11: e003. https://doi.org/10.48130/git-0024-0004.